Scheme to equilibrate the Hall response of topological systems from coherent dynamics

Yong Xu[1,*] and Ying Hu[2,3]

[1]*Center for Quantum Information, IIIS, Tsinghua University, Beijing 100084, People's Republic of China*

[2]*State Key Laboratory of Quantum Optics and Quantum Optics Devices, Institute of Laser Spectroscopy, Shanxi University, Taiyuan, Shanxi 030006, China*

[3]*Collaborative Innovation Center of Extreme Optics, Shanxi University, Taiyuan, Shanxi 030006, China*

(Received 2 August 2018; revised manuscript received 4 May 2019; published 20 May 2019)

Two-dimensional topologically distinct Chern insulators are separated by gap closing points, which exist as Weyl points in three-dimensional momentum space. Slowly varying parameters in the two-dimensional Hamiltonian across two distinct phases therefore necessarily experience the gap closing process, which prevents the intrinsic physical observable, the Hall response, from equilibrating. Here we demonstrate a scheme to equilibrate the quantized Hall response from pure coherent dynamics as the Hamiltonian is slowly tuned from the topologically trivial to nontrivial regimes. We further apply our method to Weyl semimetals in three dimensions and find the equilibrated Hall response despite the underlying gapless band structure. Our finding not only lays the theoretical foundation for observing the Hall response in Chern insulators but also for observing and controlling Weyl semimetals in ultracold atomic gases.

DOI: 10.1103/PhysRevB.99.174309

I. INTRODUCTION

At present there are significant interests and ongoing efforts in investigating out-of-equilibrium topological systems [1–25]. The motivation behind this is twofold. First, nonequilibrium topological systems can exhibit properties beyond the conventional theoretical framework classifying topological systems in equilibrium [7–25]. Second, in the context of highly coherent ultracold atoms, where preparation of topological ground state is challenging, driving the system Hamiltonian across a topological phase boundary and detecting the ensuing coherent dynamics have opened perspectives and possibilities for detecting equilibrium topological phases [4–6]. Here, although the many-body wave function initialized in a topologically trivial state stays trivial at all times, there arise dynamical features corresponding uniquely to the nontrivial bulk topology of the final Hamiltonian. While dynamical detection of the ground-state phase diagrams for Chern insulators in two dimensions have recently been reported [5,6] in ultracold quantum gases, the intrinsic Hall response has not been observed there.

For Weyl semimetals [26] in three dimensions—despite rapid development in a variety of fields [27–52]—its detection in cold atom experiments remains elusive. Since current experimental approaches for dynamical detection of 2D Chern insulators do not work for Weyl semimetals, it is natural to ask whether the nonequilibrium Hall response can manifest as an unambiguous signature for detection of Weyl semimetals in ultracold atomic gases. For Weyl semimetals, the key feature is the existence of pairs of Weyl points in gapless band structures. Such points can be regarded as the topological phase-transition points between the topologically trivial and nontrivial insulators in momentum space, leading to the topologically anomalous Hall response [29,30]. Indeed, in equilibrium, the Hall response can be directly measured reflecting the topological property of Weyl semimetals. However, in cold atom experiments for realizing (preparing a topologically nontrivial ground state is a challenge) or controlling Weyl semimetals, one inevitably experiences a nonadiabatic process, due to the gapless feature of Weyl semimetals, driving the system out of equilibrium.

In this paper, we propose a scheme to equilibrate the Hall response in both two-dimensional (2D) Chern insulators and Weyl semimetals. Our approach is motivated by a series of recent studies on nonequilibrium Hall response in 2D Chern insulators, pointing out that a nonequilibrium Hall response can build up despite the nontopological state when the Hamiltonian is slowly ramped into a topological regime. A crucial problem is, however, that this Hall response cannot naturally equilibrate to a quantized value, but rather strongly and persistently oscillates, due to inevitable nonadiabatic transitions through the gap closing point [53–55]. This issue necessarily occurs for Weyl semimetals as we have found, because of the gapless band structure containing Weyl points. To equilibrate the nonequilibrium Hall response is in principle possible by engineering laser noise [53] so that the coherent superpositions of excited and ground states of the Hamiltonian is randomized, leading to pure dephasing which preserves the band occupation, but, technically, it is very challenging to achieve this for every lattice momentum. Instead, here we show that, by simply turning on an electric field with suitable strength before the Hamiltonian is ramped into the Weyl semimetal phase, an equilibrated topological nonequilibrium Hall response can quickly arise in coherent dynamics, which

*yongxuphy@tsinghua.edu.cn

 ©2019 American Physical Society

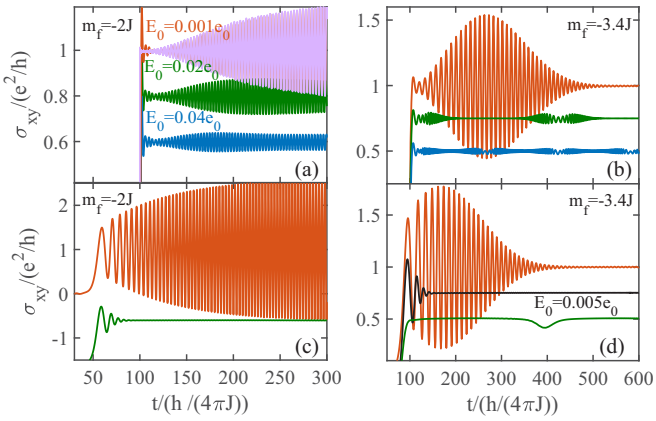

FIG. 1. Coherent dynamics of the Hall response for various strength of electric fields in two different protocols (see main text). Panels in the upper (lower) row correspond to the first (second) protocol. Here $m_i = -5J$, $v\hbar/(2J) = 0.02$, and $\tau_e = 10\hbar/(2J)$. We note that the results are similar for $\tau_e = 20\hbar/(2J)$, $30\hbar/(2J)$. For visuality, we have shifted the Hall response downward for different E_0 from an asymptotically quantized value. All curves are computed by the exact numerical method except for the pink curve in panel (a), which is calculated based on the perturbation approach. Here, $e_0 = 2J/(ea)$ is the unit of the electric field.

uniquely reflects the creation and transport of Weyl points. We stress that this phenomenon arises from a nontopological state, and is thus fundamentally different from the topological Hall response of Weyl semimetals in equilibrium.

Below, we will first illustrate the key physics underlying our scheme, taking the example of a 2D Chern insulator (see Fig. 1). Then we apply this scheme to Weyl semimetals and show how the equilibrated nonequilibrium Hall response manifests creation and time-varied separation of pairs of Weyl points, when the Hamiltonian parameter is slowly ramped across phase boundaries (see Fig. 4). As we show, our scheme not only adds an approach for equilibrating the Hall response in Chern insulators, but further sheds light on the ongoing experiments aiming at detecting Weyl semimetals and manipulating Weyl points.

II. EQUILIBRATED HALL RESPONSE OF A CHERN INSULATOR

We start by considering a Chern insulator motivated by its recent realization with ultracold atoms [56]. The relevant time-dependent Hamiltonian is $H[m_z(t)] = \sum_{\mathbf{k}} c^\dagger_{\mathbf{k}} H[\mathbf{k}, m_z(t)] c_{\mathbf{k}}$ where

$$H[\mathbf{k}, m_z(t)] = \boldsymbol{d}_{\mathbf{k}}(t) \cdot \boldsymbol{\sigma} \tag{1}$$

with $d_x = 2J\sin(k_x a)$, $d_y = 2J\sin(k_y a)$, $d_z = m_z(t) + 2J[\cos(k_x a) + \cos(k_y a)]$ at lattice momentum $\mathbf{k} = (k_x, k_y)$, J denoting the hopping strength, a being the lattice constant, $\sigma_{x,y,z}$ being the Pauli matrices, and m_z being the mass parameter corresponding to the two-photon detuning, which can be controlled in cold atom experiments. For static m_z, the ground state of the Hamiltonian is in the topologically nontrivial phase with Chern number $C = -\mathrm{sgn}[m_z/(2J)]$ for $|m_z| < 4J$, otherwise, it is in the topologically trivial phase with $C = 0$.

We will be interested in the coherent dynamics of Hall response in an experimentally relevant scenario, where the system is initially prepared in the topologically trivial ground state of the Hamiltonian $H(m_i)$ with $m_i < -4J$. We tune m_z slowly from m_i to $-4J < m_f < 0$ according to $m_z(t) = m_i + (m_f - m_i)(1 - e^{-vt})$ with velocity v. This way, the Hamiltonian $H[m_z(t)]$ changes its topology from trivial to topologically nontrivial, undergoing a transition at an energy gap closing point at critical time t_c. To probe the Hall response, at time t_e, we ramp on an electric field along x as $E_x(t) = E_0(1 - e^{-t/\tau_e})$ [57], which can be generated via a homogeneous time-dependent synthetic gauge field, i.e., $E_x(t) = \partial_t A(t)$. The Hall current along y is computed by

$$J_y(t) = \frac{e}{\hbar} \sum_{\mathbf{k}\in \mathrm{BZ}} \langle \psi_{\mathbf{k}}(t) | \partial_{k_y} H[\mathbf{k}'(t), m_z(t)] | \psi_{\mathbf{k}}(t) \rangle, \tag{2}$$

where $|\psi_{\mathbf{k}}(t)\rangle$ denotes the instantaneous wave function at momentum $\mathbf{k}$, and the summation is over the first Brillouin zone (BZ). Note that the presence of electric field induces a shift in momentum via $\mathbf{k}'(t) = [k_x + eA(t)/\hbar, k_y]$. The Hall response is thus given by $\sigma_{xy}(t) = J_y(t)/E_x(t)$, measured in units of e^2/h.

We will analyze and compare the coherent dynamics of Hall response in two different protocols for controlling the electric field: (1) We first vary the mass parameter without electric field $E_x(t)$. Then, some time after the transition of the system through the critical point at time t_c, the $E_x(t)$ is turned on, i.e., $t_e \gg t_c$. (2) The $E_x(t)$ is turned on before the modulations of m_z, i.e., $t_e \ll t_c$. The numerical results for the coherent dynamics of Hall response in both protocols are shown in Fig. 1.

We find that, while a Hall response dynamically builds up after the Hamiltonian is ramped into a topologically nontrivial regime, its equilibration to a topologically quantized value under coherent evolution crucially depends on two elements for both protocols: (i) dispersion of the energy band of the final Hamiltonian $H(m_f)$, and (ii) the magnitude of E_0. In more detail, for $m_f = -2J$ [Figs. 1(a) and 1(c)], where the corresponding energy band is flat along k_x for $k_y = 0$ [see Fig. 2(a)], we see that the Hall response cannot reach equilibrium but rather exhibits strong and persistent oscillations for $E_0/e_0 \ll v\hbar/2J$ in both protocols [see red curves for $E_0 = 0.001e_0$ with $e_0 = 2J/(ea)$ being the unit of the electric field], as also found earlier [53–55]. Remarkably, when E_0 is increased to be comparable to the ramp velocity (e.g., see green curves for $E_0 = 0.02e_0$), such irregularities disappear after a few oscillations in protocol (2), as opposed to its counterpart in protocol (1) where the oscillations are only moderately suppressed. When the underlying energy band becomes increasingly dispersive [see Fig. 2(b)], such as for $m_f = -3.4J$ [Figs. 1(b) and 1(d)], we see that the oscillations of the Hall response generically damps out at long times (but shorter than the time scale for Bloch oscillations) even for weak E_0 in both protocols, and increasing E_0 can significantly reduce the time for equilibration. These findings show that an equilibrated asymptotically quantized Hall response can build up from coherent dynamics, despite the nonadiabatic passage through the gap closing.

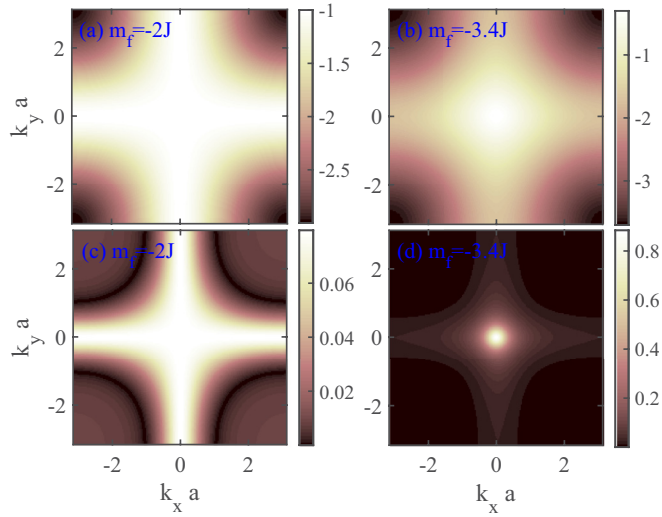

FIG. 2. Energy spectra of the lower band of the Hamiltonian (1) with $m_z(t) = m_f$ for (a) $m_f = -2J$ and (b) $m_f = -3.4J$. The unit of energy is $2J$. The Berry curvature $\Omega_-(\mathbf{k})$ for (c) $m_f = -2J$ and (d) $m_f = -3.4J$.

To gain insight into above dynamical behavior of Hall response, we first analyze protocol (1) using the perturbation approach. In this case, the energy gap closes at momentum $\mathbf{k}_c = (0, 0)$ at time t_c. Then at time t_e when $E_x(t)$ is turned on, for simplicity and to capture the essential physics, we assume that $H(m_f)$ has been reached and the state can be described by $|\psi_{\mathbf{k}}(t_e)\rangle = \sqrt{1-p(\mathbf{k})}e^{iD_1(\mathbf{k})}|u_-(\mathbf{k})\rangle + e^{i\theta(\mathbf{k})}e^{-iD_1(\mathbf{k})}\sqrt{p(\mathbf{k})}|u_+(\mathbf{k})\rangle$ for $\mathbf{k} \neq 0$, where $|u_{+(-)}(\mathbf{k})\rangle$ denotes the excited (ground) state of $H(\mathbf{k}, m_f)$, $\theta(\mathbf{k})$ is the relative phase, and $D_1(\mathbf{k}) = \int_0^{t_e} \epsilon_+[\mathbf{k}, m_z(t')]dt'/\hbar$ is the dynamical phase with $\epsilon_{+(-)}[\mathbf{k}, m_z(t)]$ ($\epsilon_+ = -\epsilon_-$) the eigenenergy of Hamiltonian $H[\mathbf{k}, m_z(t)]$. Moreover, $p(\mathbf{k})$ denotes the number of excitations created during the nonadiabatic passage through the gap closing. At times $t > t_e$, where the gap has been reopened, using time-dependent perturbation theory [58], the evolution of $|u_\lambda(\mathbf{k})\rangle$ can be approximated by $|\Phi_\lambda(\mathbf{k}', t)\rangle = e^{-i\int_{t_e}^{t}\epsilon_\lambda(\mathbf{k}')dt'/\hbar}e^{i\gamma_\lambda(t)} \times [|u_\lambda(\mathbf{k}')\rangle - ieE_x(t)\frac{\langle u_{\bar{\lambda}}(\mathbf{k}')|\partial_{k_x}|u_\lambda(\mathbf{k}')\rangle}{2\lambda\epsilon_+(\mathbf{k}')}|u_{\bar{\lambda}}(\mathbf{k}')\rangle]$ for $|E_x(t)| > 0$. Here $\bar{\lambda} \neq \lambda$ and $\gamma_\lambda(t)$ is associated with the Berry phase in the λ band. Therefore, after ramping on the electric field, the state evolves from $|\psi_{\mathbf{k}}(t_e)\rangle$ into $|\psi_{\mathbf{k}}(t > t_e)\rangle = \sqrt{1-p(\mathbf{k})}e^{iD_1(\mathbf{k})}|\Phi_-(\mathbf{k}', t)\rangle + e^{i\theta(\mathbf{k})}e^{-iD_1(\mathbf{k})}\sqrt{p(\mathbf{k})}|\Phi_+(\mathbf{k}', t)\rangle$. Substitution of this ansatz into Eq. (2) then gives the Hall current, which well captures the dynamical behavior of Hall response at times $t > t_e$, as evidenced by the pink curve in Fig. 1(a), which almost exactly overlaps the red one.

The Hall current contains three contributions, i.e.,

$$J_y(t) = J_{\text{Hall}}(t) + J_{\text{Dis}}(t) + J_{\text{Osc}}(t). \tag{3}$$

Here, $J_{\text{Hall}}(t) = [e^2E_x(t)/\hbar]\sum_{\mathbf{k}}[1-2p(\mathbf{k})]\Omega_-(\mathbf{k}')$ describes the weighted anomalous Hall current which has topological origin, with Ω_- labeling the instantaneous Berry curvature for the lower band of $H(\mathbf{k}', m_f)$. In the limit of vanishing ramp velocity, $J_{\text{Hall}}(t)/E_x(t)$ approaches the Chern number of $H(m_f)$ besides a unit. The current $J_{\text{Dis}} = (e/\hbar)\sum_{\mathbf{k}}[1-2p(\mathbf{k})]\partial_{k_y}\epsilon_-(\mathbf{k}')$ arises from the weighted band velocity, which exactly vanishes because of the underlying symmetry in our system, i.e., $\epsilon_\lambda(k_x, k_y) = \epsilon_\lambda(k_x, -k_y)$. The current $J_{\text{Osc}}(t)$ comes from the coherent superpositions between the upper and lower bands, i.e.,

$$J_{\text{Osc}}(t) = \text{Re}\left[\sum_{\mathbf{k}}\sqrt{p_{\mathbf{k}}(1-p_{\mathbf{k}})}e^{i[\theta(\mathbf{k})-D_2(\mathbf{k}')]}\Gamma(t)\right], \tag{4}$$

where Re takes the real part of an expression, $D_2(\mathbf{k}') = 2\int_{t_e}^{t} dt'\epsilon_+(\mathbf{k}')/\hbar$, and $\Gamma(t) = \frac{2e}{\hbar}e^{-2iD_1(\mathbf{k})}e^{i(\gamma_+-\gamma_-)}(g_{12} - 2ieE_x(t)h_{12}\frac{\partial_{k_y}\epsilon_+(\mathbf{k}',m_f)}{2\epsilon_+(\mathbf{k}',m_f)})$ with $g_{12}(\mathbf{k}') = \langle u_-(\mathbf{k}')|\partial_{k_y}H(\mathbf{k}', m_f)|u_+(\mathbf{k}')\rangle$, and $h_{12} = \langle\partial_{k_x}u_-(\mathbf{k}')|u_+(\mathbf{k}')\rangle$. Obviously, $J_{\text{Osc}}(t)$ is responsible for the oscillation as we detail below.

Equation (4) allows us to understand the effect of electric field on the oscillations and their damping in the coherent dynamics of Hall response as shown in Figs. 1(a) and 1(b). In our analysis we will focus on the term involving g_{12} while ignoring that involving h_{12}, which is small due to gapped energy as is numerically verified. For a slow ramp, the excitations occur in a very narrow region near the gap-closing point at $\mathbf{k}_c = (0, 0)$, which can be described in the context of Landau-Zener (LZ) physics that gives $p(\mathbf{k}) \approx e^{-4\pi J^2k^2a^2/(v_{\text{LZ}}\hbar)}$, with $v_{\text{LZ}} = (m_f + 4J)v$. Hence the dominant contribution to $J_{\text{Osc}}(t)$ comes from the momenta $k < k_c = \sqrt{v_{\text{LZ}}\hbar/(4\pi J^2a^2)}$. In this regime, in the limit of weak electric field $E_0 \to 0$, one can expand g_{12} in terms of A on the time scale $\tau_e < t \ll k_c/(eE_0)$, and the main contribution to $J_{\text{Osc}}(t)$ comes from the first term, i.e., $g_{12} \propto A = E_0(t - t_e - \tau_e)$, where the electric field is supposed to approach a constant value. Therefore, for sufficiently weak electric field such as in $E_0 = 0.001e_0$, the amplitude of oscillating Hall response will always undergo an initial increase with time [see Figs. 1(a) and 1(b)].

In the long-time limit when $k_c/(E_0e) \ll t < 2\pi\hbar/(eE_0a)$, which is quickly fulfilled as in the case when $E_0 = 0.02e_0$, we find that the oscillations persist for $m_f = -2J$ while they can be damped out for $m_f \neq -2J$ as shown in Figs. 1(a) and 1(b). The damping is caused by the significant difference for the energy spectrum $\epsilon_+(\mathbf{k}')$ along the k_x direction, which is strongly modified by the presence of large $A(t)$. To gain some intuitive understanding, let us keep only the dominant term responsible for the strong damping, $D_2(\mathbf{k}')$, and approximate $J_{\text{Osc}}(t)$ by $J_{\text{Osc}}(t) \sim 2\text{Re}\int d\mathbf{k}\sqrt{p(\mathbf{k})(1-p(\mathbf{k}))}e^{2i\epsilon_-(\mathbf{k}+\mathbf{k}_e,m_f)t'/\hbar}$ with $t' = t - t_e$, where we have taken the leading term $g_{12} \approx 2Ja$ and ignored the time-independent phase contribution and the Berry phase, which is irrelevant due to its small variation in momentum space. To see the effect of spectrum difference, let us fix $\mathbf{k}_e$ (which is driven by the electric field by $k_{ex} = eE_0t'/\hbar$), e.g., $k_{ex}a = \pi/2$, where dispersion exhibits the largest derivative along k_x for $k_y = 0$ and $|m_f| \neq 2J$. We find that the oscillations decays exponentially for $m_f = -3J$ and $v\hbar/(2J) = 0.02$. However, when $m_f = -2J$, we find $J_{Osc} \sim \sqrt{ct'}/(1 - ict')$ with $c = v_{LZ}/(\pi J)$ in the long-time limit, which decays very slowly, almost leading to a persistent oscillation, consistent with Fig. 1(a), because of flat energy dispersion for $k_y = 0$. Interestingly, we further see that the oscillations of Hall currents revive as it approaches a period of $2\pi\hbar/(eE_0a)$ because Bloch oscillation occurs [see blue curve in Fig. 1(b)]. This also implies that the oscillations of Hall

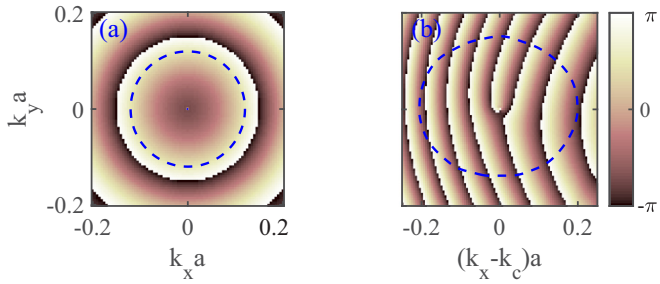

FIG. 3. Profiles of $\theta(\mathbf{k})$ near the gap closing point $\mathbf{k}_c$ (for $\mathbf{k} \neq \mathbf{k}_c$) for (a) protocol (1) with $k_c = 0$, and (b) protocol (2) with $k_c = -eA(t_c)/\hbar$ and $E_0 = 0.02e_0$. At momenta depicted by the dashed blue line, the corresponding population in the excited state is 0.1.

currents cannot be completely damped out if the relevant time scale for damping is $>\pi\hbar/(eE_0a)$.

The above analysis guides our intuition into the remarkably equilibrated Hall response in protocol (2). As $E_x(t)$ is present initially before $m_z(t)$ is varied, the energy gap closing point is shifted to $\mathbf{k}_c = [-eA(t_c)/\hbar, 0]$. This motivates us to consider the form of Eq. (4) with the replacement $p(\mathbf{k}) \to p(\mathbf{k}-\mathbf{k}_c)$ and $\theta(\mathbf{k}) \to \theta(\mathbf{k}-\mathbf{k}_c)$. When $E_0 = 0.02e_0$, we find that $\theta(\mathbf{k}-\mathbf{k}_c)$ exhibits rapid variations near $\mathbf{k}_c$ along the x direction [see Fig. 3(b) calculated by the exact numerical method], in sharp contrast to the counterpart of protocol (1) [see Fig. 3(a)], where $\theta(\mathbf{k})$ varies slowly. The rapid variations introduce the strong damping when the integration over momentum space is performed, leading to a rapid equilibration of Hall response in protocol (2) reflecting the topology of the instantaneous Hamiltonian, even for $m_f = -2J$.

In Fig. 1(d), we also observe that the green curve exhibits a conspicuous dip around $t = 395\hbar/(2J)$. To explain this phenomenon, we plot the profiles of the Berry curvature for the lower band $\Omega_-(\mathbf{k})$ [$\Omega_-(\mathbf{k}) = -\Omega_+(\mathbf{k})$] in the (k_x, k_y) plane. We see that the Berry curvature is uniformly distributed along k_x around $k_y = 0$ for $m_f = -2J$, while, for $m_f = -3.4J$, it is localized around $\mathbf{k} = 0$. Since the electric field is ramped up initially, we have $J_{\rm Hall}(t) = (e^2E_0/\hbar)\sum_{\mathbf{k}}[1-2p(\mathbf{k}-\mathbf{k}_c)]\Omega_-[k_x - k_{cx} + eE_0(t-t_c)/\hbar, k_y]$ with $\mathbf{k}_c = [k_{cx}, k_{cy}] = [-eA(t_c)/\hbar, 0]$, implying that the Hall response experiences a conspicuous decline when $eE_0(t-t_c)/\hbar = 2n\pi/a$ with n being an integer for $m_z = -3.4J$.

III. EQUILIBRATED HALL RESPONSE OF WEYL SEMIMETALS

Let us consider a system of atoms in a 3D lattice described by the Hamiltonian (see Appendix B for its realization scheme)

$$H_C = \frac{\mathbf{p}^2}{2m} - \sum_{v=x,y,z} V_v \cos^2(k_{Lv}r_v) + m_z\sigma_z + V_{\rm SO}, \qquad (5)$$

where m is the mass of atoms, $\mathbf{p}$ is the momentum operator, $V_{\rm SO} = M_y\sigma_x - M_x\sigma_y$ describes the nondiagonal optical lattices with $M_x = \Omega_{\rm SO}\sin(k_{Lx}r_x)\cos(k_{Ly}r_y)\cos(k_{Lz}r_z)$ and $M_y = \Omega_{\rm SO}\sin(k_{Ly}r_y)\cos(k_{Lx}r_x)\cos(k_{Lz}r_z)$, and $V_{x,y,z} > 0$ denotes the strength of diagonal lattices with the period $a_v = \pi/k_{Lv}$. Hamiltonian (5) can be recast into the following tight-binding form (see Appendix B for derivation), i.e., $H_{\rm TB} = \sum_{\mathbf{x}}[-\sum_v(J_v\hat{c}^\dagger_{\mathbf{x}}\hat{c}_{\mathbf{x}+a_v\mathbf{e}_v} + \text{H.c.}) + m_z\hat{c}^\dagger_{\mathbf{x}}\sigma_z\hat{c}_{\mathbf{x}} + (-1)^{j_x+j_y+j_z}J_{\rm SO}(\hat{c}^\dagger_{\mathbf{x}}\sigma_y\hat{c}_{\mathbf{x}+a_x\mathbf{e}_x} - \hat{c}^\dagger_{\mathbf{x}}\sigma_x\hat{c}_{\mathbf{x}+a_y\mathbf{e}_y} + \text{H.c.})]$. Here $\hat{c}^\dagger_{\mathbf{x}} = (\hat{c}^\dagger_{\mathbf{x}\uparrow} \quad \hat{c}^\dagger_{\mathbf{x}\downarrow})$ with $\hat{c}_{\mathbf{x}\sigma}$ ($\hat{c}^\dagger_{\mathbf{x}\sigma}$) annihilating (creating) an atom with spin σ at $\mathbf{x} = \sum_v j_v a_v \mathbf{e}_v$. The corresponding Hamiltonian in momentum space reads

$$H_{\rm 3D}(\mathbf{k}) = m_z\sigma_z - h_t\tau_x + \tau_y(d_y\sigma_x - d_x\sigma_y), \qquad (6)$$

where τ_v denotes the Pauli matrix describing the sublattices, $h_t = -2\sum_{v=x,y,z}J_v\cos(k_va_v)$, $d_x = 2J_{\rm SO}\sin(k_xa_x)$ and $d_y = 2J_{\rm SO}\sin(k_ya_y)$. The eigenenergy corresponding to Hamiltonian (6) is $E_\pm(\lambda) = \pm\sqrt{d_x^2 + d_y^2 + (h_t - \lambda m_z)^2}$ with $\lambda = \pm 1$. Below we will assume $J_v = J_{\rm SO} = J$ and $a_v = a$ for convenience.

The semimetal (6) exhibits a very rich phase diagram. When $|m_z| > 6J$, the Weyl semimetal is in the trivial insulating phase. When $2J < |m_z| < 6J$, the system is in the topological phase featuring one pair of Weyl points, whereas for $|m_z| < 2J$ and $m_z \neq 0$, the semimetal has two pairs of Weyl points. For $m_z = 0$, the system is the Dirac semimetal with two Dirac points [59]. The locations of Weyl points and Dirac points in momentum space are displayed in Fig. 4(a).

To characterize a Weyl point in equilibrium, one can use the Chern number of the eigenstates (or Hamiltonian) defined over a closed surface in momentum space as shown in Fig. 4(b). With a Weyl point inside, the Chern number equals ± 1. However, as we slowly modify m_z, the Chern number of states over the surface remains unchanged under unitary time evolution, even though the Weyl point defined by the Hamiltonian moves out of the surface, implying that the Chern number of states does not reflect the Chern number of the Hamiltonian in nonequilibrium scenarios (see the detailed discussion in Appendix C).

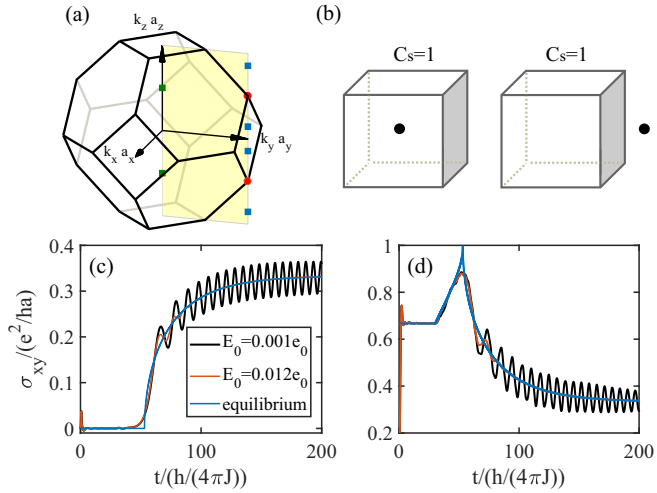

FIG. 4. (a) The first Brillouin zone with a pair of Dirac points, one and two pairs of Weyl points, denoted by the solid red circles and green and blue squares, respectively. (b) Schematics illustrating that the Chern number of states remains unchanged on a closed surface when a Weyl point moves out of the surface. Evolution of the Hall response over time as m_z varies slowly (c) from $-7J$ to $-5J$ and (d) from $-3J$ to $-J$.

Although the Chern number of states over a closed surface remains unchanged as a Hamiltonian parameter slowly varies, we find that the Hall response along y for the considered Weyl semimetal [60] changes [see Figs. 4(c) and 4(d)], when an electric field $E_x(t)$ is switched on before $m_z(t)$ is slowly tuned. Remarkably, the Hall response at $E_0 = 0.012e_0$ is finally equilibrated to the value of its equilibrium counterpart dictated by the instantaneous Hamiltonian as we slowly tune the system from a topologically trivial insulator to a Weyl semimetal phase with two Weyl points [see Fig. 4(c)] and from a phase with two Weyl points to another phase with four points [see Fig. 4(d)]; this is in sharp contrast to the case for $E_x = 0.001e_0$ where the Hall response cannot be equilibrated but rather exhibits strong oscillations, as we have discussed earlier.

In summary, we have demonstrated a scheme to equilibrate the quantized Hall response from pure coherent dynamics when a 2D insulator is ramped from a topologically trivial into nontrivial regime. We further apply our strategy to a 3D Weyl semimetal and find the equilibrated Hall response as the number and location of Weyl points are slowly tuned. Our findings not only pave the way for observing the 2D Hall response but also for detecting and controlling Weyl semimetals in ultracold atomic gases.

ACKNOWLEDGMENTS

We thank B. Wu, D.-L. Deng, Y.-K. Wu, Z.-X. Gong, T. Qin, and X.-P. Li for helpful discussions. Y.X. acknowledges support from the Tsinghua start-up program and the National Thousand-Young-Talents Program. Y.H. acknowledges support from the National Thousand-Young-Talents Program, National Natural Science Foundation of China (Grants No. 11874038 and No. 11434007), National Key Research and Development Program of China (Grant No. 2017YFA0304203), Changjiang Scholars and Innovative Research Team in University of Ministry of Education of China (No. IRT_17R70), the Fund for Shanxi "1331 Project" Key Subjects Construction, 111 Project (Grant No. D18001), and the 100-Talents Plan of Shanxi Province.

APPENDIX A: CALCULATION OF THE ELECTRIC FIELD INDUCED PHASES

To calculate the phase $\theta(\mathbf{k}+\mathbf{k}_c)$ induced by the electric field, we expand the state in the basis of instantaneous eigenstates $|u_\lambda(\mathbf{k}', m_z(t))\rangle$ as

$$|\psi_{\mathbf{k}}(t)\rangle = \sum_{\lambda=\pm} \alpha_\lambda(\mathbf{k},t)A_\lambda(\mathbf{k},t)|u_\lambda(\mathbf{k}', m_z(t))\rangle, \tag{A1}$$

where $|u_\lambda(\mathbf{k}', m_z(t))\rangle$ satisfies $H(\mathbf{k}', m_z(t))|u_\lambda(\mathbf{k}', m_z(t))\rangle = \epsilon_\lambda(\mathbf{k}', m_z(t))|u_\lambda(\mathbf{k}', m_z(t))\rangle$ with $\epsilon_\lambda(\mathbf{k}', m_z(t)) = \lambda\sqrt{\sum_{v=x,y,z} d_v^2(\mathbf{k}', m_z(t))}$ and $\lambda = \pm 1$, $A_\lambda(\mathbf{k},t) = e^{-i\int_0^t \epsilon_\lambda(\mathbf{k}', m_z(t'))dt'} e^{i\gamma_\lambda(t)}$ corresponding to the dynamical and Berry phases $\gamma_\lambda(t) = i\int_0^t dt'\langle u_\lambda(\mathbf{k}', m_z(t'))|\partial_{t'} u_\lambda(\mathbf{k}', m_z(t'))\rangle$, respectively. Plugging Eq. (A1) into the Schrödinger equation yields

$$\partial_t \alpha_- = -f(t)\alpha_+ A_+/A_-, \tag{A2}$$

$$\partial_t \alpha_+ = f(t)^* \alpha_- A_-/A_+, \tag{A3}$$

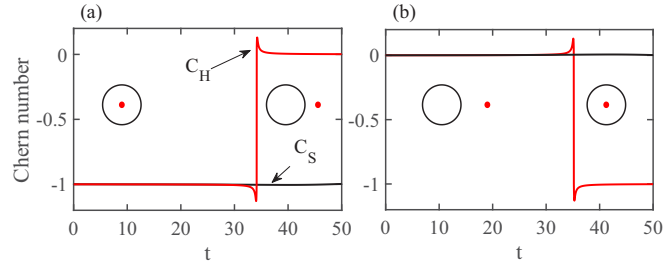

FIG. 5. Evolution of the Chern number of the Hamiltonian H'_{3D} on a closed surface in the 3D momentum space: C_H (denoted by the red line), and the Chern number of the time-evolved states on the same surface: C_S (denoted by the black line). In (a), at $t = 0$, we choose a closed surface (schematically denoted by a circle) such that there is a Weyl point (denoted by a red point) inside it. As time evolves, the Weyl point defined as the gap closing point in the instantaneous Hamiltonian moves out of the surface. In (b), the surface is chosen such that there are no Weyl points inside it at $t = 0$. As time evolves, a Weyl point travels inside the surface. Note that our numerical calculation of C_H around the sudden change region is not accurate due to the very small gap. Here the unit of time is $\hbar/(2J)$.

where $f(t) = \langle u_-(\mathbf{k}', m_z(t))|\partial_t u_+(\mathbf{k}', m_z(t))\rangle$. Supposing that all atoms are initialized to the lower band, we can calculate the time evolution of $\alpha_\lambda(\mathbf{k},t)$, obtaining $\theta(\mathbf{k}) = \text{angle}[\alpha_+(\mathbf{k}, t > t_c)/\alpha_-(\mathbf{k}, t > t_c)]$.

APPENDIX B: EXPERIMENTAL SCHEME FOR REALIZATION OF A WEYL SEMIMETAL AND DERIVATION OF THEIR TIGHT-BINDING MODEL

To implement the continuous model in Eq. (5) in the main text, we only need to slightly modify our previous scheme for realization of a dynamical 4D Weyl nodal ring [61]. We refer the reader to Figs. 3(c) and 3(d) for a laser configuration setup, where two sets of Raman laser beams are utilized to generate the off-diagonal spin-dependent optical lattices. Each set includes two pairs of Raman laser beams. In the first set, for one pair, the Rabi frequencies are $[\bar{\Omega}_1 = -\bar{\Omega}_{10}\cos(k_{Ly}r_y)e^{-ik_{Lz}r_z/2}$, $\bar{\Omega}_2 = i\bar{\Omega}_{20}\sin(k_{Lx}r_x)e^{ik_{Lz}r_z/2}]$, and for the other pair, they are $[\bar{\Omega}'_1 = -\bar{\Omega}_{10}\cos(k_{Ly}r_y)e^{ik_{Lz}r_z/2}$, $\bar{\Omega}'_2 = i\bar{\Omega}_{20}\sin(k_{Lx}r_x)e^{-ik_{Lz}r_z/2}]$. In the second set, for one pair, the Rabi frequencies are $[\tilde{\Omega}_1 = \tilde{\Omega}_{10}\sin(k_{Ly}r_y)e^{-ik_{Lz}r_z/2}$, $\tilde{\Omega}_2 = \bar{\Omega}_{10}\cos(k_{Lx}r_x)e^{ik_{Lz}r_z/2}]$, and for the other pair, they are $[\tilde{\Omega}'_1 = \tilde{\Omega}_{10}\sin(k_{Ly}r_y)e^{ik_{Lz}r_z/2}$, $\tilde{\Omega}'_2 = \bar{\Omega}_{10}\cos(k_{Lx}r_x)e^{-ik_{Lz}r_z/2}]$. We also require another laser beam to create an optical lattice along z. Using this scheme, we can achieve the Hamiltonian in Eq. (7).

To obtain the continuous model's tight-binding Hamiltonian, let us write down the many-body Hamiltonian using the field operator

$$H_{II} = \int d\mathbf{r}\hat{\psi}^\dagger(\mathbf{r})H_C\hat{\psi}(\mathbf{r}), \tag{B1}$$

where $\hat{\psi}(\mathbf{r}) = [\hat{\psi}_\uparrow(\mathbf{r}) \quad \hat{\psi}_\downarrow(\mathbf{r})]^T$ with $\hat{\psi}_\sigma(\mathbf{r})$ $[\hat{\psi}^\dagger_\sigma(\mathbf{r})]$ being a field operator destroying (creating) a particle located at $\mathbf{r}$ with spin σ ($\sigma = \uparrow, \downarrow$). The anticommutation or commutation relation $[\hat{\psi}_\sigma(\mathbf{r}), \hat{\psi}^\dagger_{\sigma'}(\mathbf{r}')]_\pm = \delta_{\sigma\sigma'}\delta(\mathbf{r}-\mathbf{r}')$ is required to be

respected for fermionic (+) or bosonic operators (−), respectively.

We approximately expand the field operator as

$$\hat{\psi}_\sigma(\mathbf{r}) \approx \sum_{\mathbf{x},\sigma} W_{\mathbf{x}}(\mathbf{r})\hat{c}_{\mathbf{x},\sigma}, \tag{B2}$$

where $\hat{c}_{\mathbf{x},\sigma}$ is the annihilation operator for a particle with spin σ located at the site $\mathbf{x}$, which satisfies the anticommutation or commutation relation $[\hat{c}_{\mathbf{x},\sigma}, \hat{c}^\dagger_{\mathbf{x}',\sigma'}]_\pm = \delta_{\mathbf{x},\mathbf{x}'}\delta_{\sigma,\sigma'}$ for fermionic (+) or bosonic (−) atoms, respectively, and $W_{\mathbf{x}}(\mathbf{r})$ is the Wannier function for the lowest band of the Hamiltonian with $h_z = V_{\mathrm{SO}} = 0$, which is located at the site $\mathbf{x} = \sum_\nu j_\nu a_\nu \mathbf{e}_\nu$ with $\nu = x, y, z$.

With the aid of Eq. (B2), we can obtain the following tight-binding Hamiltonian by keeping only the nearest-neighbor hopping terms (see Refs. [46,62] for the detailed derivation and verification for its validity):

$$\begin{aligned} H_{\mathrm{TB}} = \sum_{\mathbf{x}} \Bigg[&- \sum_\nu \left(J_\nu \hat{c}^\dagger_{\mathbf{x}} \hat{c}_{\mathbf{x}+a_\nu \mathbf{e}_\nu} + \mathrm{H.c.} \right) + m_z \hat{c}^\dagger_{\mathbf{x}} \sigma_z \hat{c}_{\mathbf{x}} \Bigg] \\ &+ \sum_{\mathbf{x}} (-1)^{j_x+j_y+j_z} J_{\mathrm{SO}} \left(\hat{c}^\dagger_{\mathbf{x}} \sigma_y \hat{c}_{\mathbf{x}+a_x \mathbf{e}_x} \right. \\ &\left. - \hat{c}^\dagger_{\mathbf{x}} \sigma_x \hat{c}_{\mathbf{x}+a_y \mathbf{e}_y} + \mathrm{H.c.} \right), \end{aligned} \tag{B3}$$

where $\hat{c}^\dagger_{\mathbf{x}} = (\hat{c}^\dagger_{\mathbf{x},\uparrow}, \hat{c}^\dagger_{\mathbf{x},\downarrow})$. In the basis of $\Psi(\mathbf{k})^\dagger = (e^{-ik_x a_x}\hat{A}^\dagger_{\mathbf{k}\uparrow} \quad e^{-ik_x a_x}\hat{A}^\dagger_{\mathbf{k}\downarrow} \quad \hat{B}^\dagger_{\mathbf{k}\uparrow} \quad \hat{B}^\dagger_{\mathbf{k}\downarrow})$ where A and B correspond to two sublattices, the Hamiltonian can be written as in momentum space $H_{\mathrm{TB}} = \sum_{\mathbf{k}} \Psi(\mathbf{k})^\dagger H_{3\mathrm{D}}(\mathbf{k}) \Psi(\mathbf{k})$, where $H_{3\mathrm{D}}(\mathbf{k})$ is the Hamiltonian (5) in the main text. Applying the transformation $\hat{a}_{\mathbf{x}\uparrow} = (-1)^{j_x+j_y+j_z}\hat{c}_{\mathbf{x}\uparrow}$ and $\hat{a}_{\mathbf{x}\downarrow} = \hat{c}_{\mathbf{x}\downarrow}$ reduces the model to the form

$$\begin{aligned} H'_{\mathrm{TB}} = \sum_{\mathbf{x}} \Bigg[&\sum_\nu \left(J_\nu \hat{a}^\dagger_{\mathbf{x}} \sigma_z \hat{a}_{\mathbf{x}+a_\nu \mathbf{e}_\nu} + \mathrm{H.c.} \right) + m_z \hat{a}^\dagger_{\mathbf{x}} \sigma_z \hat{a}_{\mathbf{x}} \\ &- J_{\mathrm{SO}} \left(i\hat{a}^\dagger_{\mathbf{x}} \sigma_y \hat{a}_{\mathbf{x}+a_y \mathbf{e}_y} + i\hat{a}^\dagger_{\mathbf{x}} \sigma_x \hat{a}_{\mathbf{x}+a_x \mathbf{e}_x} + \mathrm{H.c.} \right) \Bigg], \end{aligned} \tag{B4}$$

where $\hat{a}^\dagger_{\mathbf{x}} = (\hat{a}^\dagger_{\mathbf{x},\uparrow}, \hat{a}^\dagger_{\mathbf{x},\downarrow})$. The lattice structure becomes simple orthorhombic from a rocksalt lattice structure. Using the Fourier transformation, we can write this Hamiltonian in momentum space as $H'_{\mathrm{TB}} = \sum_{\mathbf{k}} \hat{a}^\dagger_{\mathbf{k}} H'_{3\mathrm{D}}(\mathbf{k}) \hat{a}_{\mathbf{k}}$, where $\hat{a}^\dagger_{\mathbf{k}} = (\hat{a}^\dagger_{\mathbf{k},\uparrow}, \hat{a}^\dagger_{\mathbf{k},\downarrow})$ and $H'_{3\mathrm{D}}(\mathbf{k})$ is given in Ref. [60].

APPENDIX C: CHANGE OF THE CHERN NUMBER OF THE STATES AND THE HAMILTONIAN

Let us choose a closed surface $\mathcal{S}$ parametrized by (u_1, u_2) in momentum space and calculate the evolution of the Chern number of the states and the Hamiltonian $H'_{3\mathrm{D}}$ on the surface. The Chern number is defined by [63,64]

$$C = \frac{1}{4\pi} \oint_{\mathcal{S}} \mathbf{d} \cdot \left(\frac{\partial \mathbf{d}}{\partial u_1} \times \frac{\partial \mathbf{d}}{\partial u_2} \right) du_1 du_2. \tag{C1}$$

To determine the Chern number of the Hamiltonian C_H, we take $\mathbf{d} = \sum_{\nu=x,y,z} \hat{d}_\nu \mathbf{e}_\nu$ with $d_z = -h_t + m_z$ and $\hat{d}_\nu = d_\nu / \sqrt{d_x^2 + d_y^2 + d_z^2}$; for the Chern number of states C_S, we take $\mathbf{d} = -\langle \psi_{u_1,u_2}(t) | \boldsymbol{\sigma} | \psi_{u_1,u_2}(t) \rangle$, where $\boldsymbol{\sigma} = \sum_{\nu=x,y,z} \sigma_\nu \mathbf{e}_\nu$ and $|\psi_{u_1,u_2}(t)\rangle$ denotes the instantaneous wave function on the surface with the ground state chosen as the initial wave function. In Fig. 5, we plot the evolution of C_H and C_S for two different scenarios. In the first case, we choose a closed surface so that it encloses a Weyl point at $t = 0$ and, as time evolves, the Weyl point moves out of the surface. We find that the Chern number of states over the surface remains unchanged while the Chern number of the Hamiltonian changes to zero, once the point moves out of the surface. In the second case, the surface is initially chosen so that there are no Weyl points inside it. As we slowly tune a Hamiltonian parameter so that a Weyl point moves inside the surface, we find that during this process the Chern number of states remains zero while the Chern number of the Hamiltonian changes to -1. This demonstrates that the states cannot reflect the change of a Weyl point in a Hamiltonian due to the out-of-equilibrium feature.

[1] G. Jotzu, M. Messer, R. Desbuquois, M. Lebrat, T. Uehlinger, D. Greif, and T. Esslinger, Nature (London) **515**, 237 (2014).

[2] N. Fläschner, B. Rem, M. Tarnowski, D. Vogel, D.-S. Lühmann, K. Sengstock, and C. Weitenberg, Science **352**, 1091 (2016).

[3] Z. Wu, L. Zhang, W. Sun, X.-T. Xu, B.-Z. Wang, S.-C. Ji, Y. Deng, S. Chen, X.-J. Liu, and J.-W. Pan, Science **354**, 83 (2016).

[4] M. Tarnowski, F. N. Ünal, N. Fläschner, B. S. Rem, A. Eckardt, K. Sengstock, and C. Weitenberg, Nat. Commun. **10**, 1728 (2019).

[5] N. Fläschner, D. Vogel, M. Tarnowski, B. S. Rem, D.-S. Lühmann, M. Heyl, J. C. Budich, L. Mathey, K. Sengstock, and C. Weitenberg, Nat. Phys. **14**, 265 (2018).

[6] W. Sun, C.-R. Yi, B.-Z. Wang, W.-W. Zhang, B. C. Sanders, X.-T. Xu, Z.-Y. Wang, J. Schmiedmayer, Y. Deng, X.-J. Liu, S. Chen, and J.-W. Pan, Phys. Rev. Lett. **121**, 250403 (2018).

[7] L. D. Alessio and M. Rigol, Nat. Commun. **6**, 8336 (2015).

[8] M. D. Caio, N. R. Cooper, and M. J. Bhaseen, Phys. Rev. Lett. **115**, 236403 (2015).

[9] J. C. Budich and M. Heyl, Phys. Rev. B **93**, 085416 (2016).

[10] P. Wang, M. Schmitt, and S. Kehrein, Phys. Rev. B **93**, 085134 (2016).

[11] J. H. Wilson, J. C. W. Song, and G. Refael, Phys. Rev. Lett. **117**, 235302 (2016).

[12] M. D. Caio, N. R. Cooper, and M. J. Bhaseen, Phys. Rev. B **94**, 155104 (2016).

[13] F. N. Ünal, E. J. Mueller, and M. Ö. Oktel, Phys. Rev. A **94**, 053604 (2016).

[14] Y. Ge and M. Rigol, Phys. Rev. A **96**, 023610 (2017).

[15] C. Wang, P. Zhang, X. Chen, J. Yu, and H. Zhai, Phys. Rev. Lett. **118**, 185701 (2017).

[16] C. Yang, L. Li, and S. Chen, Phys. Rev. B **97**, 060304(R) (2018).

[17] M. Heyl and J. C. Budich, Phys. Rev. B **96**, 180304(R) (2017).

[18] M. Schüler and P. Werner, Phys. Rev. B **96**, 155122 (2017).
[19] A. Kruckenhauser and J. C. Budich, Phys. Rev. B **98**, 195124 (2018).
[20] L. Ulčakar, J. Mravlje, A. Ramšak, and T. Rejec, Phys. Rev. B **97**, 195127 (2018).
[21] L. Zhang, L. Zhang, S. Niu, and X.-J. Liu, Sci. Bull. **63**, 1385 (2018).
[22] L. Asteria, D. T. Tran, T. Ozawa, M. Tarnowski, B. S. Rem, N. Fläschner, K. Sengstock, N. Goldman, and C. Weitenberg, Nat. Phys. **15**, 449 (2019).
[23] J. Yu, Phys. Rev. A **99**, 043619 (2019).
[24] Z. Gong and M. Ueda, Phys. Rev. Lett. **121**, 250601 (2018).
[25] X. Qiu, T.-S. Deng, G.-C. Guo, and W. Yi, Phys. Rev. A **98**, 021601 (2018).
[26] N. P. Armitage, E. J. Mele, and A. Vishwanath, Rev. Mod. Phys. **90**, 015001 (2018).
[27] G. E. Volovik, *The Universe in a Helium Droplet* (Clarendon, Oxford, 2003).
[28] X. Wan, A. M. Turner, A. Vishwanath, and S. Y. Savrasov, Phys. Rev. B **83**, 205101 (2011).
[29] K.-Y. Yang, Y.-M. Lu, and Y. Ran, Phys. Rev. B **84**, 075129 (2011).
[30] A. A. Burkov and L. Balents, Phys. Rev. Lett. **107**, 127205 (2011).
[31] G. Xu, H. Weng, Z. Wang, X. Dai, and Z. Fang, Phys. Rev. Lett. **107**, 186806 (2011).
[32] M. Gong, S. Tewari, and C. Zhang, Phys. Rev. Lett. **107**, 195303 (2011).
[33] L. Lu, L. Fu, J. D. Joannopoulos, and M. Soljačić, Nat. Photon. **7**, 294 (2013).
[34] Y. Xu, R.-L. Chu, and C. Zhang, Phys. Rev. Lett. **112**, 136402 (2014).
[35] S. A. Yang, H. Pan, and F. Zhang, Phys. Rev. Lett. **113**, 046401 (2014).
[36] T. Dubček, C. J. Kennedy, L. Lu, W. Ketterle, M. Soljačić, and H. Buljan, Phys. Rev. Lett. **114**, 225301 (2015).
[37] B. Liu, X. Li, L. Yin, and W. V. Liu, Phys. Rev. Lett. **114**, 045302 (2015).
[38] H. Weng, C. Fang, Z. Fang, B. A. Bernevig, and X. Dai, Phys. Rev. X **5**, 011029 (2015).
[39] S.-Y. Xu, I. Belopolski, N. Alidoust, M. Neupane, C. Zhang, R. Sankar, S.-M. Huang, C.-C. Lee, G. Chang, B. Wang, G. Bian, H. Zheng, D. S. Sanchez, F. Chou, H. Lin, S. Jia, and M. Z. Hasan, Science **349**, 613 (2015).
[40] B. Q. Lv, H. M. Weng, B. B. Fu, X. P. Wang, H. Miao, J. Ma, P. Richard, X. C. Huang, L. X. Zhao, G. F. Chen, Z. Fang, X. Dai, T. Qian, and H. Ding, Phys. Rev. X **5**, 031013 (2015).
[41] L. Lu, Z. Wang, D. Ye, L. Ran, L. Fu, J. D. Joannopoulos, and M. Soljačić, Science **349**, 622 (2015).
[42] X. Li and S. D. Sarma, Nat. Commun. **6**, 7137 (2015).
[43] Y. Xu, F. Zhang, and C. Zhang, Phys. Rev. Lett. **115**, 265304 (2015).
[44] H. Ishizuka, T. Hayata, M. Ueda, and N. Nagaosa, Phys. Rev. Lett. **117**, 216601 (2016).
[45] W.-Y. He, S. Zhang, and K. T. Law, Phys. Rev. A **94**, 013606 (2016).
[46] Y. Xu and L.-M. Duan, Phys. Rev. A **94**, 053619 (2016).
[47] Z. Yan and Z. Wang, Phys. Rev. Lett. **117**, 087402 (2016).
[48] C.-K. Chan, P. A. Lee, K. S. Burch, J. H. Han, and Y. Ran, Phys. Rev. Lett. **116**, 026805 (2016).
[49] H. Hübener, M. A. Sentef, U. D. Giovannini, A. F. Kemper, and A. Rubio, Nat. Commun. **8**, 13940 (2017).
[50] L.-J. Lang, S.-L. Zhang, K. T. Law, and Q. Zhou, Phys. Rev. B **96**, 035145 (2017).
[51] Y.-B. Yang, T. Qin, D.-L. Deng, L.-M. Duan, and Y. Xu, arXiv:1810.07710.
[52] Y. Xu, Front. Phys. **14**, 43402 (2019).
[53] Y. Hu, P. Zoller, and J. C. Budich, Phys. Rev. Lett. **117**, 126803 (2016).
[54] A. Dauphin, D.-T. Tran, M. Lewenstein, and N. Goldman, 2D Mater. **4**, 024010 (2017).
[55] L. P. Gavensky, G. Usaj, and C. A. Balseiro, Phys. Rev. B **98**, 165414 (2018).
[56] W. Sun, B.-Z. Wang, X.-T. Xu, C.-R. Yi, L. Zhang, Z. Wu, Y. Deng, X.-J. Liu, S. Chen, and J.-W. Pan, Phys. Rev. Lett. **121**, 150401 (2018).
[57] M. Aidelsburger, M. Lohse, C. Schweizer, M. Atala, J. T. Barreiro, S. Nascimbène, N. R. Cooper, I. Bloch, and N. Goldman, Nat. Phys. **11**, 162 (2015).
[58] D. Xiao, M.-C. Chang, and Q. Niu, Rev. Mod. Phys. **82**, 1959 (2010).
[59] The Dirac points can be clearly seen from the transformed Hamiltonian in a partitioned diagonal form: $H(\mathbf{k}) = \tau_z[-h_t\sigma_z + d_x\sigma_x + d_y\sigma_y] + m_z\sigma_z\tau_0$.
[60] For simplicity, we perform a transformation $\hat{a}_{\mathbf{x}\uparrow} = (-1)^{j_x+j_y+j_z}\hat{c}_{\mathbf{x}\uparrow}$ and $\hat{a}_{\mathbf{x}\downarrow} = \hat{c}_{\mathbf{x}\downarrow}$, giving a simpler Hamiltonian in momentum space, $H'_{3D}(\mathbf{k}) = (-h_t + m_z)\sigma_z + d_x\sigma_x + d_y\sigma_y$, which has the same form as the 2D Hamiltonian (1), regarding k_z as a parameter.
[61] Y.-B. Yang, L.-M. Duan, and Y. Xu, Phys. Rev. B **98**, 165128 (2018).
[62] Y. Xu and C. Zhang, Phys. Rev. A **93**, 063606 (2016).
[63] M. Kleman and O. D. Lavrentovich, *Soft Matter Physics: An Introduction* (Springer, New York, 2003).
[64] Y. Xu, S.-T. Wang, and L.-M. Duan, Phys. Rev. Lett. **118**, 045701 (2017).